Radiation Measurements 153 (2022) 106745

Contents lists available at ScienceDirect

Radiation Measurements

journal homepage: www.elsevier.com/locate/radmeas

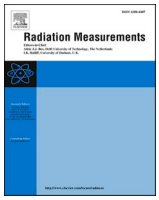

Numerical modeling of radiation-induced charge neutralization in MOS devices

L. Sambuco Salomone [a,*], M. Garcia-Inza [a,c], S. Carbonetto [a,c], J. Lipovetzky [b,c,d], E. Redin [a], A. Faigón [a,c]

[a] Laboratorio de Física de Dispositivos - Microelectrónica, Facultad de Ingeniería, Universidad de Buenos AiresAv, Paseo Colón 850, Ciudad Autónoma de Buenos Aires, Argentina
[b] Instituto Balseiro, Bariloche, R8402, Argentina
[c] Consejo Nacional de Investigaciones Científicas y Técnicas, Buenos Aires, Argentina
[d] Comisión Nacional de Energía Atómica, Buenos Aires C1429BNP, Argentina

ARTICLE INFO

keywords:
MOSFETs
MOS dosimetry
Numerical modeling

ABSTRACT

Radiation-induced charge neutralization at different bias is studied for 230 nm p-channel MOS dosimeters under γ-radiation. A physics-based numerical model is employed to reproduce the experimental results. Good agreement is obtained between measurements and simulations considering capture and neutralization rates independent of electric field during neutralization stages. Sensitivity curves during neutralization stages show a two part process consisting of a slow decrease for short times followed by a rapid fall. Remarkably, the model predicts this behavior and allows to understand that in terms of the potential well generated due to trapped holes within the oxide.

1. Introduction

When a metal-oxide-semiconductor (MOS) structure is irradiated, positive charge buildup (PCB) occurs within the gate oxide as a consequence of the capture of radiation-generated holes into preexisted defects, such as oxygen vacancies. This oxide charge distorts the electric field, leading to a negative shift in the threshold voltage (V_t) of MOS transistors. The amount of charge trapped in the oxide depends on the bias applied during the irradiation. In particular, when a positive bias is applied on the gate at the initial stage of an irradiation and then it is switched to a zero or negative voltage, the trapped holes attract radiation-generated electrons, which once captured neutralize the positive charge, restoring the trap to its initial neutral state and leading to a recovery of V_t towards its pre-irradiation value in a process known as radiation-induced charge neutralization (RICN) (Fleetwood, 1990).

Given its radiation sensitivity, MOS devices can be employed as dosimeters with the V_t value as the sensed variable that provides information about the absorbed dose (García Moreno et al., 2009; Siebel et al., 2015; Li et al., 2014; Lipovetzky et al., 2013; Vasović and Ristić, 2012). In this context, switched-bias irradiations are particularly useful because they allow to restore V_t, at least partially. This opposite behavior for positive and negative biases makes possible the alternation between both to keep V_t within a predefined window avoiding the saturation of the response, as demonstrated in bias controlled cycled measurements (BCCM) (Faigón et al., 2008; Lipovetzky et al., 2010). As V_t-shift with dose depends on applied bias, the response of the device during RICN must be characterized to determine which is the better bias condition for maximizing sensitivity.

The modeling of total ionizing dose (TID) effects on MOS structures was approached with different levels of complexity, ranging from analytical expressions for the evolution of V_t with dose (Pavan et al., 1994; Lenahan and Conley, 1998a), to the numerical resolution of a set of equations including the main physical processes behind the generation and trapping of charge within the oxide (Boesch et al., 1986; Sánchez Esqueda et al., 2011; Barnaby et al., 2009; Krantz et al., 1987). Recently, we presented a physics-based numerical model (Sambuco Salomone et al., 2015, 2016; Cassani et al., 2021), and it was shown that under switched-bias irradiations, the charge redistribution within the oxide plays a key role in explaining a wide variety of phenomena.

In this work, we present new experimental data of 230 nm thick oxide p-channel MOS dosimeters exposed to switched-bias irradiations with a γ-ray source to explore the bias dependence of radiation-induced

* Corresponding author.
E-mail address: lsambuco@fi.uba.ar (L. Sambuco Salomone).

https://doi.org/10.1016/j.radmeas.2022.106745
Received 10 December 2021; Received in revised form 21 February 2022; Accepted 14 March 2022
Available online 17 March 2022
1350-4487/© 2022 Elsevier Ltd. All rights reserved.

charge neutralization. Also, numerical simulations are employed to understand the experimental sensitivity curves which shows a complex pattern not reported before.

The paper is organized as follows. Section II summarizes the theory and implementation of the numerical model. The main results are presented in Section III, whereas several issues are discussed in Section IV. Finally, Section V presents the conclusions.

2. Physics-based numerical model

2.1. Theory

The model deals with the main physical mechanisms leading to positive charge accumulation within the gate oxide during irradiation, as shown in Fig. 1. A brief description of the model is provided in this section. For further details, the reader can consult (SambucoSalomone et al., 2015; Cassani et al., 2021).

When radiation interacts with a MOS device, electron-hole pairs (ehp) are generated within the oxide. Only a fraction of them escapes initial recombination. This fractional yield (Y) is strongly dependent on electric field. For the experiments modeled in this work, Dozier expression for ^{60}Co is considered (Dozier et al., 1987).

The carriers remaining flow is driven by the electric field. Field dependent electron mobility is included in the model through an expression that fits Hughes experiments (Hughes, 1975). Holes move dispersively (Curtis and Srour, 1977; McLean et al., 1976), but at room temperature and usual dose levels, the intrinsic hole mobility can be used (Vasudevan and Vasi, 1993).

Holes within the oxide can be captured by defects (Lenahan and Dressendorfer, 1984; Kim and Lenahan, 1988; Nicklaw et al., 2002). When an electron is close to a trapped hole, there is a probability of neutralization. Both hole capture and neutralization are treated as proportional to the free carrier density.

The system of equations to be solved is the following,

$$\frac{dn_f}{dt} = -\frac{dj_n}{dx} + R_g - R_n n_f p_t \tag{1}$$

$$\frac{dp_f}{dt} = -\frac{dj_p}{dx} + R_g - R_c p_f (P_t - p_t) \tag{2}$$

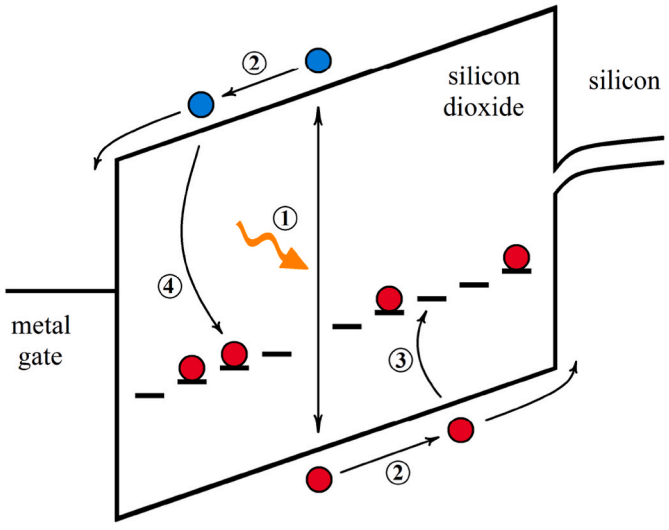

Fig. 1. Band diagram schematic representation of the physical model for a MOS structure with positive gate bias. ① charge generation and initial recombination, ② electron and hole transport, ③ hole trapping, and ④ trapped hole neutralization through electron trapping.

$$\frac{dp_t}{dt} = R_c p_f (P_t - p_t) - R_n n_f p_t \tag{3}$$

$$\frac{dF}{dx} = -\frac{q}{\varepsilon_{ox}} (p_t + p_f - n_f) \tag{4}$$

where n_f and p_f are the densities of free electrons and holes, respectively, p_t is the density of trapped holes, P_t is the density of traps, R_c and R_n are the trapping and neutralization rates, respectively. The generation rate is $R_g = g_0 Y D_r$, where $g_0 = 8.1 \times 10^{14}$ cm^{-3}Gy^{-1} and D_r is the dose rate. x is referred to the Si/SiO$_2$ interface. F is the electric field, q is the elementary charge and ε_{ox} is the SiO$_2$ permittivity ($3.9\varepsilon_0$). The electron (j_n) and hole (j_p) fluxes are described by the usual drift-diffusion model.

The V_t-shift due to changes in the oxide charge is calculated using,

$$\Delta V_t = -\frac{q}{\varepsilon_{ox}} \int_0^{t_{ox}} p_t (t_{ox} - x) dx \tag{5}$$

where t_{ox} is the oxide thickness, and free carriers were neglected due to their much lower concentrations relative to the trapped charge.

2.2. Numerical implementation

For the numerical simulation of equations (1)–(4), time derivatives were replaced by discretized finite-difference approximations, using the implicit Euler method. This leads to a system of nonlinear equations, which was solved using the full Newton method. In each time step, the iteration ends when the residual of the nonlinear system is lower than a chosen accuracy value. To reduce the condition number of the Jacobian matrix, variables were scaled taking into account the much different order of magnitude of electron and hole mobilities.

For the spatial discretization, the symmetric Franceschetti scheme (Franceschetti and Macdonald, 1979) was implemented to reduce the number of mesh points without compromising the accuracy ($N = 50$, $\theta = 0.1$). In order to reduce the computational time, an automatic time step control was employed, based on the local truncation error. To avoid numerical instabilities due to the coupling between Poisson and continuity equations, the Scharfetter-Gummel expressions were used to describe the electron and hole fluxes (Scharfetter and Gummel, 1969).

Regarding the fitting procedure, as the density of hole traps P_t and capture R_c and neutralization R_n rates are supposed to depend on fabrication conditions (Conley et al., 1997; Lenahan and Conley, 1998b), these are the model fitting parameters. However, as the density of trapped holes is much lower than the density of available traps ($p_t \ll P_t$) for all doses, the product $P_t R_c$ arises as a single effective fitting parameter. We arbitrarily choose uniformly distributed hole traps with density $P_t = 10^{19}$ cm^{-3}, leaving R_c and R_n as free parameters.

3. Simulation of experimental results

The devices exposed to radiation were 230 nm thick oxide commercial-off-the-shelf p-channel MOSFET. Fig. 2 shows the transfer characteristic (I_D vs. V_G) for a virgin device.

The devices were irradiated with a ^{60}Co γ-radiation source, with a dose rate of 2.19 Gy/s. Measurements were carried out by sampling the threshold voltage V_t during irradiation using a special hardware designed for this application. This instrument switches between two operation modes, as shown in Fig. 3. For most of the time, the system is in biasing mode where a voltage V_G is applied to the gate with other terminals grounded. When a V_t sample is required, the system switches to reading mode, in which a reference current is imposed in the diode-connected transistor, and the gate-to-source voltage is measured.

Fig. 4 presents the experimental results of a switched-bias irradiation showing successive PCB and RICN stages. The device was pre-irradiated to lower V_t in order to study charge neutralization. During RICN stages,

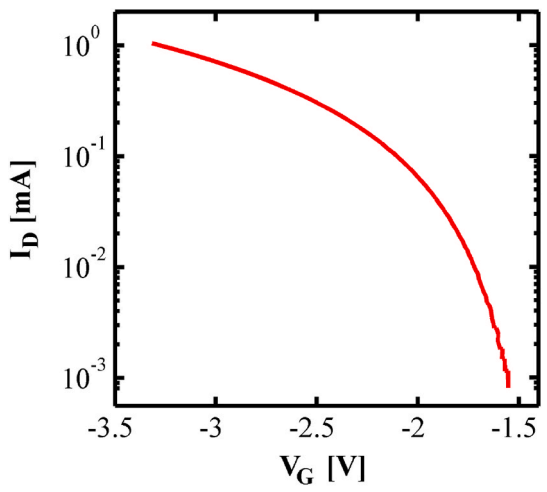

Fig. 2. I_D vs. V_G characteristic for a virgin device.

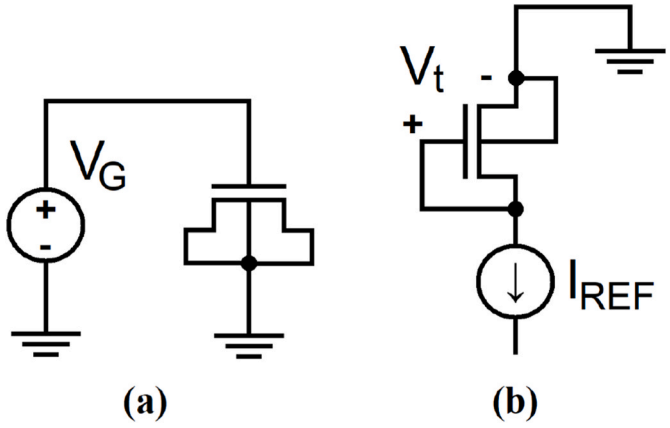

Fig. 3. Simplified schematics of the circuit during (a) biasing mode, and (b) reading mode.

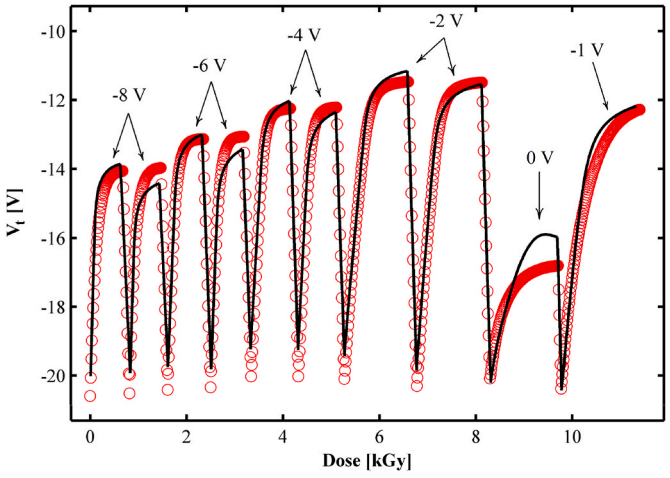

Fig. 4. Experimental (symbols) and simulated (line) V_t vs. dose curves for a switched bias experiment (V_G = 8 V for all PCB stages).

V_t recovers until saturation with a steady-state V_t value depending on V_G, which is fairly reproduced by the model. Between successive RICN stages the bias was switched to V_G = 8 V to lower V_t again. During RICN stages, capture and neutralization rates were $R_c = 10^{-13}$ cm^{3}s^{-1}, and $R_n = 10^{-8}$ cm^{3}s^{-1}, respectively. To fit the V_t descent during PCB stages a higher capture rate $R_c = 10^{-12}$ cm^{3}s^{-1} was needed.

Fig. 5 shows a comparison between the experimental and simulated sensitivity along the irradiation for three RICN stages at different biases. A common feature is observed in all of them: sensitivity slowly decreases at the beginning of RICN up to a point beyond which it falls down rapidly. As the bias is more negative, the initial sensitivity increases even when the steady-state V_t value is lower. Remarkably, the model predicts all of this.

To understand the physical origin of the sensitivity pattern during RICN stages, Fig. 6(a) shows the band diagram as extracted from simulations at the beginning of the second RICN stage at $V_G = -2$ V, whereas Fig. 6(b) shows the trapped holes distribution at different times during the same stage. As the positive charge within the oxide is higher than that corresponding to the steady-state at the given bias, a potential well is formed. Electrons generated all over the oxide are drifted towards the bottom of the potential well where they neutralize trapped holes. As time passes, the potential well vanishes, and a steady-state is reached. It is worth noting that as the potential well confines the electrons, it is indistinguishable whether they actually recombine with trapped holes, or their presence just compensates the positive charge. That explains why RICN is almost neutralization rate independent when it is mainly driven by the presence of the potential well, as we previously observed for FOXFET dosimeters at zero bias (Cassani et al., 2021). Hence, as long as the potential well remains, sensitivity will slowly drop, consistent with the first part of the RICN stages shown in Fig. 5. Once the well fades away, the sensitivity drops abruptly, evidencing that a steady-state is reached, and consistent with the second part of the RICN stages.

In addition to the general explanation given above, the experimental results and the simulations showed that as the bias is more negative, the initial sensitivity increases, whereas the dose needed to make the potential well vanish decreases. To explain these features, the electronic energy across the oxide layer at the beginning of the RICN stage is shown in Fig. 7 with the bias as parameter. As shown, the more negative the bias, the higher the electric fields, which implies that more charge is effectively generated (more pairs escape from initial recombination), so a higher initial sensitivity value is achieved. At the same time, as the bias is more negative, the potential well is shallower, so it takes less to disappeared due to charge neutralization.

4. Discussion

The first point worth discussing is the electric field dependence of capture and neutralization rates. As shown in this work, the response of the dosimeter during RICN stages at different biases can be reproduced with single values for capture and neutralization rates. This result is

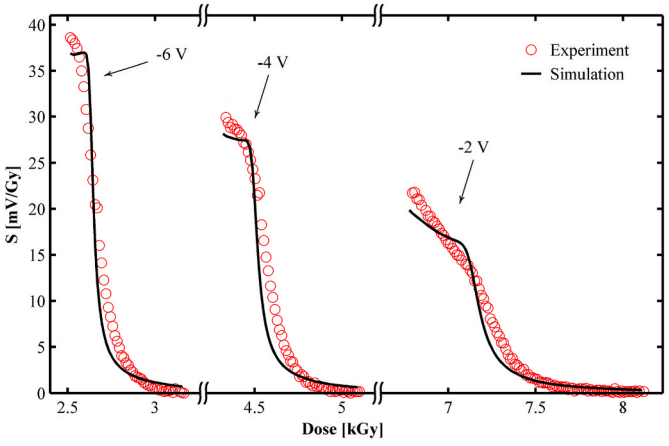

Fig. 5. Experimental (symbols) and simulated (lines) radiation sensitivities as a function of dose for several RICN stages shown in Fig. 4.

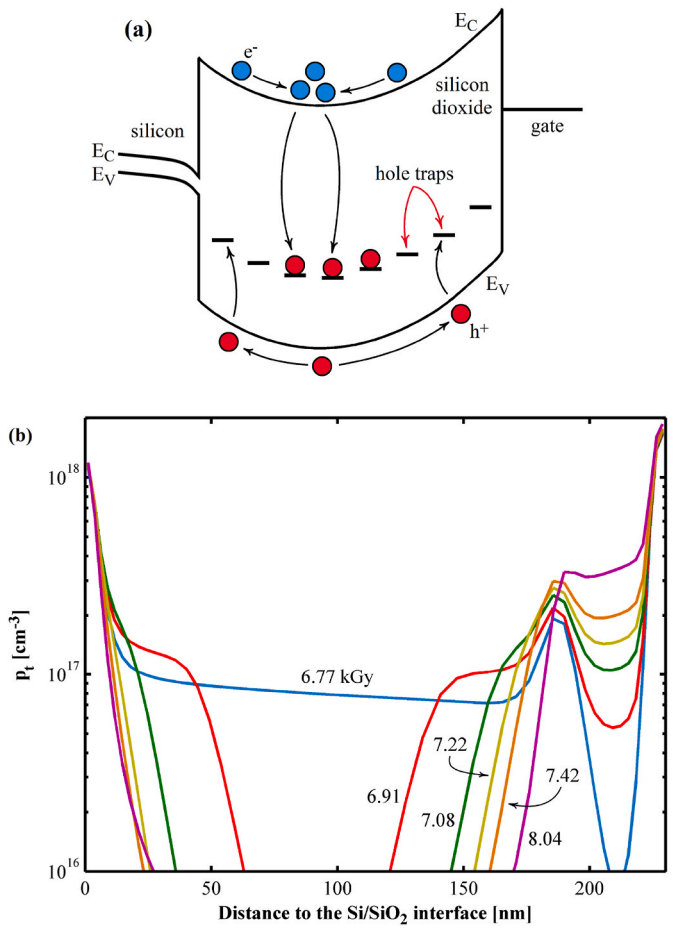

Fig. 6. (a) Simulated band diagram at the beginning of the second RICN stage at $V_G = -2$ V, and (b) trapped holes distribution within the oxide at different times during the same RICN stage.

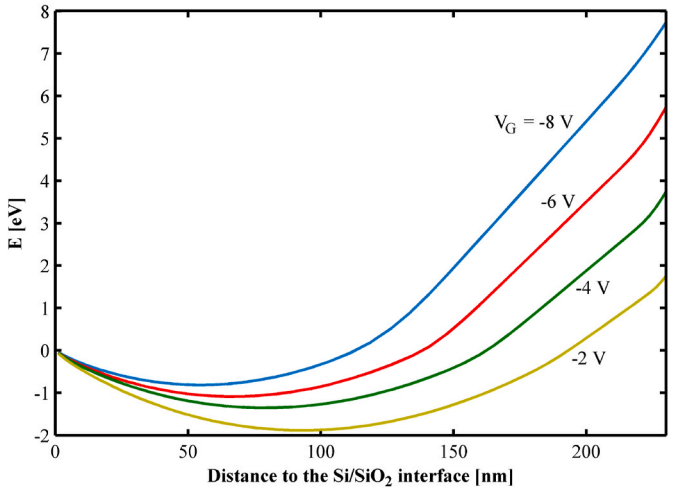

Fig. 7. Electronic energy across the oxide layer at the beginning of RICN stages with different biases.

especially remarkable as the model not only fairly reproduces the V_t vs. dose curves, but also the sensitivity ones. As mentioned above, RICN stages has two distinguishable parts: (i) the sensitivity slowly decreases until absorbed dose reaches a critical value beyond which (ii) the sensitivity falls down rapidly. As the RICN bias is more negative, the initial sensitivity increases, whereas the first part becomes shorter. The model was quite good in predicting both trends, which suggests that the dependence of the RICN response with applied bias is mainly dominated by the electric field dependence of the initial recombination and carriers transport, and not by an electric field dependence of capture and/or neutralization rates, which however cannot be ruled out. This issue deserves further study.

In bias-controlled cycled measurements (BCCM) the biases during PCB and RICN stages determine the corresponding sensitivities. However, if the V_t window is relatively wide, it is not accurate to assume a constant sensitivity for each stage. To analyze this issue, Fig. 8 shows the measured sensitivity values as a function of V_t during the RICN stages for different biases. As observed, if more negative bias voltages are chosen, the average sensitivity during the RICN stage could be increased, but at the cost of a higher variability. In that sense, the results presented in this work shows that if both bias voltage and V_t window are carefully chosen, it is possible that the sensor operates in the first part of the RICN response, where its sensitivity is relatively stable as the neutralization process is driven by the presence of the potential well within the oxide, as discussed above.

5. Conclusions

The response of 230 nm p-channel MOS dosimeters exposed to switched-bias irradiation was presented, and the bias dependence of the radiation-induced charge neutralization stages were studied. The sensitivity curves during RICN stages showed a first part where sensitivity slowly decreases with absorbed dose, followed by a second part where it drops down rapidly to zero as saturation of V_t-shift was reached.

A physics-based numerical model was employed to reproduce the experimental results by adjusting the value of capture and neutralization rates. Good agreement was obtained between experiments and simulations. The model predicted the experimentally observed two parts in the sensitivity curves during RICN, together with the dependence on bias of the initial sensitivity, and the dose beyond which sensitivity falls rapidly.

The implications the results presented here have for dosimetry applications were discussed with particular emphasis on bias-controlled cycled measurements, showing that a careful choice of the bias during neutralization stages is mandatory to achieve good sensitivity and low variability.

Declaration of competing interest

The authors declare that they have no known competing financial

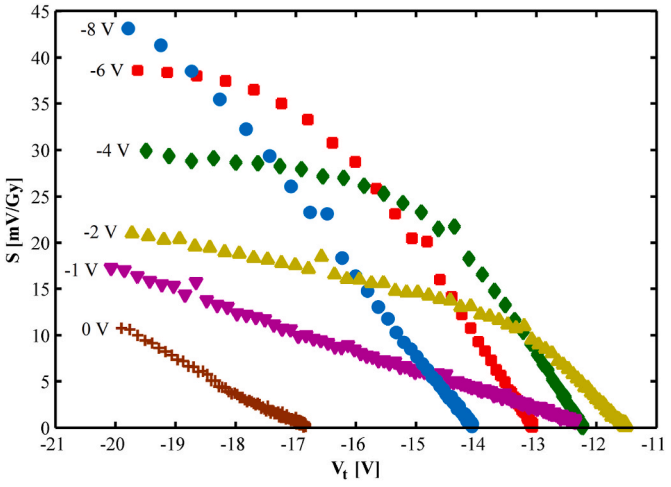

Fig. 8. Sensitivity during RICN stages as a function of V_t for different bias voltages from experiments in Fig. 4.

interests or personal relationships that could have appeared to influence the work reported in this paper.

Acknowledgment

This work was supported by grants UBACyT 20020190200002BA and 20020170100685BA.

The authors want to thank to the Planta de Irradiación Semi Industrial (PISI), Comisión Nacional de Energía Atómica (CNEA), for the access to irradiation facilities.

References

Barnaby, H.J., McLain, M.L., Sánchez Esqueda, I., Chen, X.J., 2009. Modeling ionizing radiation effects in solid state materials and CMOS devices. IEEE Trans. Circ. Syst.: Regular Pap. 56 (8), 1870–1883.

Boesch, H.E., McLean, F.B., Benedetto, J.M., McGarrity, J.M., 1986. Saturation of threshold voltage shift in MOSFET's at high total dose. IEEE Trans. Nucl. Sci. 33 (6), 1191–1197.

Cassani, M.V., Sambuco Salomone, L., Carbonetto, S., Faigón, A., Redin, E., Garcia-Inza, M., 2021. Experimental characterization and numerical modeling of total ionizing dose effects on field oxide MOS dosimeters. Radiat. Phys. Chem. 182, 109338.

Conley Jr., J.F., Lenahan, P.M., Wallace, B.D., Cole, P., 1997. Quantitative model of radiation induced charge trapping in SiO_2. IEEE Trans. Electron. Dev. 44 (6), 1804–1809.

Curtis, O.L., Srour, J.R., 1977. The multiple-trapping model and hole transport in SiO_2. J. Appl. Phys. 48 (9), 3819–3828.

Dozier, C.M., Fleetwood, D.M., Brown, D.B., Winokur, P.S., 1987. An evaluation of low-energy X-ray and cobalt-60 irradiations of MOS transistors. IEEE Trans. Nucl. Sci. 34 (6), 1535–1539.

Faigón, A., Lipovetzky, J., Redin, E., Krusczenski, G., 2008. Extension of the measurement range of MOS dosimeters using radiation induced charge neutralization. IEEE Trans. Nucl. Sci. 55 (4), 2141–2147.

Fleetwood, D.M., 1990. Radiation-induced charge neutralization and interface-trap buildup in metal-oxide-semiconductor devices. J. Appl. Phys. 67 (1), 580–583.

Franceschetti, D.R., Macdonald, J.R., 1979. Numerical analysis of electrical response: statics and dynamics of space-charge regions at blocking electrodes. J. Appl. Phys. 50 (1), 291–302.

García Moreno, E., Picos, R., Isern, E., Roca, M., Bota, S., Suenaga, K., 2009. Radiation sensor compatible with standard CMOS technology. IEEE Trans. Nucl. Sci. 56 (5), 2910–2915.

Hughes, R.C., 1975. Hot electrons in SiO_2. Phys. Rev. Lett. 35 (7), 449–452.

Kim, Y.Y., Lenahan, P.M., 1988. Electron-spin-resonance study of radiation-induced paramagnetic defects in oxides grown on (100) silicon substrates. J. Appl. Phys. 64 (7), 3551–3557.

Krantz, R.J., Aukerman, L.W., Zietlow, T.C., 1987. Applied field and total dose dependence of trapped charge buildup in MOS devices. IEEE Trans. Nucl. Sci. 35 (6), 1196–1201.

Lenahan, P.M., Conley, J.F., 1998a. A comprehensive physically based predictive model for radiation damage in MOS systems. IEEE Trans. Nucl. Sci. 45 (6), 2413–2423.

Lenahan, P.M., Conley Jr., J.F., 1998b. A comprehensive physically based predictive model for radiation damage in MOS systems. IEEE Trans. Electron. Dev. 45 (6), 2413–2423.

Lenahan, P.M., Dressendorfer, P.V., 1984. Hole traps and trivalent silicon centers in metal/oxide/silicon devices. J. Appl. Phys. 55 (10), 3495–3499.

Li, Y., Porter, W.M., Kshirsagar, C., Roth, I., Su, Y., Reynolds, M.A., Gerbi, B.J., Koester, S.J., 2014. Fully-depleted silicon-on-insulator devices for radiation dosimetry in cancer therapy. IEEE Trans. Nucl. Sci. 61 (6), 3443–3450.

Lipovetzky, J., Redin, E.G., García Inza, M.A., Carbonetto, S., Faigón, A., 2010. Reducing measurement uncertainties using bias cycled measurement in MOS dosimetry at different temperatures. IEEE Trans. Nucl. Sci. 57 (2), 848–853.

Lipovetzky, J., García Inza, M.A., Carbonetto, S., Carra, M.J., Redin, E., Sambuco Salomone, L., Faigón, A., 2013. Field oxide n-channel MOS dosimeters fabricated in CMOS processes. IEEE Trans. Nucl. Sci. 60 (6), 4683–4691.

McLean, F.B., Boesch, H.E., McGarrity, J.M., 1976. Hole transport and recovery characteristics of SiO_2 gate insulators. IEEE Trans. Nucl. Sci. 23 (6), 1506–1512.

Nicklaw, C.J., Lu, Z.-Y., Fleetwood, D.M., Schrimpf, R.D., Pantelides, S.T., 2002. The structure, properties, and dynamics of oxygen vacancies in amorphous SiO_2. IEEE Trans. Nucl. Sci. 49 (6), 2667–2673.

Pavan, P., Tu, R.H., Minami, E.R., Lum, G., Ko, P.K., Hu, C., 1994. A complete radiation reliability software simulator. IEEE Trans. Nucl. Sci. 41 (6), 2619–2630.

Sambuco Salomone, L., Faigón, A., Redin, E.G., 2015. Numerical modeling of MOS dosimeters under switched bias irradiations. IEEE Trans. Nucl. Sci. 62 (4), 1665–1673.

Sambuco Salomone, L., Holmes-Siedle, A., Faigón, A., 2016. Long term effects of charge redistribution in cycled bias operating MOS dosimeter. IEEE Trans. Nucl. Sci. 63 (6), 2997–3002.

Sánchez Esqueda, I., Barnaby, H.J., Adell, P.C., Rax, B.G., Hjalmarson, H.P., McLain, M. L., Pease, R.L., 2011. Modeling low dose rate effects in shallow trench isolation oxides. IEEE Trans. Nucl. Sci. 58 (6), 2945–2952.

Scharfetter, D.L., Gummel, H.K., 1969. Large-signal analysis of a silicon read diode oscillator. IEEE Trans. Electron. Dev. 16 (1), 64–77.

Siebel, O.F., Pereira, J.G., Souza, R.S., Ramirez-Fernandez, F.J., Schneider, M.C., Galup-Montoro, C., 2015. A very-low-cost dosimeter based on the off-the-shelf CD4007 MOSFET array for in vivo radiotherapy applications. Radiat. Meas. 75, 53–63.

Vasović, N.D., Ristić, G.S., 2012. A new microcontroller-based RADFET dosimeter reader. Radiat. Meas. 47, 272–276.

Vasudevan, V., Vasi, J., 1993. A simulation of the multiple trapping model for continuous time random walk transport. J. Appl. Phys. 74 (5), 3224–3230.